Journal of Molecular Catalysis A: Chemical 293 (2008) 8–16

Contents lists available at ScienceDirect

Journal of Molecular Catalysis A: Chemical

journal homepage: www.elsevier.com/locate/molcata

Production of hydrogen via partial oxidation of methanol over bimetallic Au–Cu/TiO_2 catalysts

Ti-Cheng Ou, Feg-Wen Chang*, L. Selva Roselin

Department of Chemical and Materials Engineering, National Central University, Chungli 32001, Taiwan

ARTICLE INFO

Article history:
Received 7 March 2008
Received in revised form 23 June 2008
Accepted 26 June 2008
Available online 6 July 2008

Keywords:
Au–Cu bimetallic catalyst
TiO_2 support
Partial oxidation of methanol
Hydrogen
Deposition–precipitation

ABSTRACT

The catalytic activity of Au/TiO_2 (2 wt.% Au), Cu/TiO_2 (2 wt.% Cu) and Au–Cu/TiO_2 (1 wt.% Au–1 wt.% Cu) catalysts were studied for partial oxidation of methanol (POM) to produce H_2. The catalysts were characterized by ICP-AES, XRD, TEM, TPR and XPS analyses. The bimetallic Au–Cu/TiO_2 catalysts are more active, stable and exhibit higher hydrogen selectively with smaller amount of CO compared to the monometallic Au/TiO_2 and Cu/TiO_2 catalysts. The enhanced activity, selectivity and stability of the bimetallic catalysts are due to Au–Cu interaction that creates smaller metal particles, which consequently stabilize the active component for POM to produce hydrogen. The activity of Au–Cu/TiO_2 catalysts at different pH during preparation, calcination temperature and reaction temperature were optimized. The Au–Cu/TiO_2 catalysts prepared at pH 7 and dried at 373 K show higher activity. The catalytic performance at various reaction temperatures shows that the methanol conversion and hydrogen selectivity are increased with rise in temperature. The CO selectivity is increased beyond 548 K. Other possible reactions involved during POM are suggested as methanol combustion, steam reforming, decomposition, reverse water gas shift, water gas shift and CO oxidation.

1. Introduction

Fuel cells are expected to play a major role in the future for their high efficiency and low emission of pollutants. In particular, polymer electrolyte fuel cell (PEFC) systems using hydrogen as an energy source have attracted much attention due to their low operating temperature [1]. Methanol has been recommended as the best source for hydrogen fuel among the high energy density liquid fuels. Methanol can be converted to hydrogen by several reactions, including methanol steam reforming [2,3], partial oxidation of methanol [4–6], oxidative methanol reforming [7] and methanol decomposition [8]. Partial oxidation of methanol (POM) offers the advantages of an exothermic reaction with high reaction rates (Eq. (1)):

$$CH_3OH + (1/2)O_2 \rightarrow 2H_2 + CO_2; \quad \Delta H^{\circ}_{298} = -192.5\ \text{kJ/mol} \qquad (1)$$

Supported copper, palladium, platinum and gold have been reported as catalysts for hydrogen generation from methanol by POM. Copper containing catalysts [6,9,10] give similar results as supported palladium catalysts [4,5]. The main disadvantage of these catalysts is formation of considerable amount of carbon monoxide, which deactivates the precious Pt electrode. The interests in nano-sized gold supported catalysts are extremely increased due to their high activity in different reactions at low temperatures [11]. The use of these catalysts for POM showed that these catalysts can produce CO-free hydrogen [12]. Several studies demonstrate that activity and stability of the gold catalyst increased if it is supported on, or promoted by, transition-metal oxides [13–18]. For instance, Au/Al_2O_3 catalyst modified by copper oxide exhibited high catalytic activity in CO oxidation [13]. Lin et al. [14] studied the effect of different oxidic additives such as Cu, Fe, Ce, Li and Ti on the activity of Au/Al_2O_3 catalysts for ammonia oxidation. Of these additives, copper showed higher activity and selectivity towards the desired product. The addition of Cu or copper oxide to Au catalyst was studied for several other reactions including water gas shift (WGS) [15], total oxidation of methane, ethane and propane [16] and epoxidation of propene [17]. In composite catalysts, two different materials complement each other in electronic properties, oxygen mobility and surface stability [18].

In the present study, the interaction of Au and Cu in Au–Cu/TiO_2 bimetallic catalyst was investigated. For this, the catalytic activity of bimetallic Au–Cu/TiO_2 catalyst was compared with its corresponding monometallic Au/TiO_2 and Cu/TiO_2 catalysts for POM to produce H_2. In addition, the experimental parameters such as pH during preparation of the catalyst, calcination temperature and reaction temperature on the activity of Au–Cu/TiO_2 catalysts were optimized. We employed several techniques to identify the surface morphology, composition, oxidation state and crystallite size

* Corresponding author. Tel.: +886 3 4227151x34202; fax: +886 3 4252296.
E-mail address: fwchang@cc.ncu.edu.tw (F.-W. Chang).

1381-1169/$ – see front matter © 2008 Elsevier B.V. All rights reserved.
doi:10.1016/j.molcata.2008.06.017

by inductively coupled plasma atomic emission spectroscopy (ICP-AES), X-ray diffraction (XRD), transmission electron microscopy (TEM), X-ray photoelectron spectroscopy (XPS) and temperature-programmed reduction (TPR) analyses.

2. Experimental

2.1. Catalyst preparation

Au/TiO_2 (2 wt.% Au), Cu/TiO_2 (2 wt.% Cu) and $Au–Cu/TiO_2$ (1 wt.% Au, 1 wt.% Cu) catalysts with a total metal loading of 2 wt.% were prepared by deposition–precipitation method [12], using tetrachloroauric acid ($HAuCl_4{\cdot}3H_2O$, 99.99%, Alfa Aesar), copper nitrate pentahemihydrate ($Cu(NO_3)_2{\cdot}2.5H_2O$, Riedel-deHaën) and TiO_2 (Degussa P25, BET surface area 50 m^2/g). Typically, an aqueous solution of $HAuCl_4{\cdot}3H_2O$ and/or $Cu(NO_3)_2{\cdot}2.5H_2O$ were mixed together with stirring at 343 K. The pH was adjusted to the desired value by the addition of small amounts of 0.1N NaOH. This was followed by the addition of the TiO_2 support material. The slurry was then aged at 343 K for 2 h. The precipitates were filtered and washed carefully until all chloride ions were removed. The samples were dried in air at 373 K for 24 h and finally calcined in air at different temperatures for 4 h.

2.2. Catalyst characterization

The bulk amount of gold and copper in the catalysts were quantified by ICP-AES using a Jobin Yvon JY-24 spectrometer. A portion of 0.02 g of catalyst was dissolved by aqua regia (HNO_3:HCl, in 1:3 ratio) and then microwaved for 15 min. The solution was cooled down and diluted within the detection limit of the instrument.

XRD measurement was performed using a Bruker D8A X-ray diffractometer operated at 40 kV and 30 mA using Cu Kα radiation with a wavelength of 1.5406 Å. The scanning angle was from 10° to 70° at a rate of 0.02°/s.

TEM analysis was performed on a JEOL JEM-2000FX II, instrument operated at 160 kV. The sample preparation was described in detail elsewhere [19]. From each sample, about one hundred Au and Cu particles were measured carefully in order to determine a justified average particle size and size distribution.

XPS technique was performed to determine the chemical state of surface Au and Cu in $Au–Cu/TiO_2$ catalyst at different conditions. The measurements were carried out on a Thermo VG Scientific Sigma Probe spectrometer using monochromatized Al Kα radiation (1486.6 eV). The binding energies were determined utilizing by C 1s spectrum as reference at 285 eV.

The TPR experiment was performed in a U-shaped microreactor made of quartz, surrounded with a furnace controlled by a programming heating system. Prior to the TPR experiment, 40 mg of the catalyst sample was pretreated under flowing Ar (50 ml/min) at 373 K for 45 min. After the pretreatment, the sample was cooled to room temperature. A reducing gas composed of 5% H_2 plus 95% Ar was employed at a flow rate of 50 ml/min, with a heating ramp of 10 K/min from 323 to 673 K. The amount of hydrogen consumed was determined by gas chromatography (GC) equipped with a thermal conductivity detector (TCD).

2.3. Catalytic activity measurements

Partial oxidation of methanol was carried out using an apparatus, which has been described in detail elsewhere [12]. The reaction was carried out at atmospheric pressure and at temperatures between 473 and 598 K, using a U-shaped microreactor made of quartz (i.d. = 4 mm). The reactor was located in a programmable furnace with a type K thermocouple placed in the center of the catalyst bed. The Ar and O_2 were transported by Brooks 5850E mass flow meters with a precision controller (Protec Instrument Co. Ltd., Model: PC-540) to control the total flow rate at 60 ml/min. The molar composition of methanol in the feed was 392 μmol/min, and the molar ratio of O_2/CH_3OH was kept at 0.3 with a gas hourly space velocity (GHSV) of 48,000 h^{-1}. The reaction products were analyzed on-line by two gas chromatographs (GC) with thermal conductivity detectors equipped with porapak Q and carbosieve S-II columns.

3. Results and discussion

3.1. Metal loading at various pH during preparation of the catalyst

Elemental analysis of the samples was determined to verify the gold and copper content at various pH values during preparation of $Au–Cu/TiO_2$ catalysts. With nominal loadings of 1 wt.% Au and 1 wt.% Cu, the fraction of these metals deposited on the support at various pH values during the preparation of the catalysts are listed in Table 1. A maximum deposition of gold was observed at pH 7 with 0.98 wt.%. At the same time, complete deposition of copper was observed at pH values between 7 and 8. The fraction of gold deposited on the support obviously decreased at pH 8. The deposition of metals on the support is governed by the composition of metal species in solution at various pH values and charge of the support material at various pH values. The composition of the gold and copper species in solution is pH dependent. The extent of hydrolysis of metal species increases with rise in pH. The main species

Table 1
Surface properties of Au/TiO_2 (2 wt.% Au), Cu/TiO_2 (2 wt.% Cu) and $Au–Cu/TiO_2$ (1 wt.% Au, 1 wt.% Cu) catalysts

Catalyst	pH	Calcination temperature (K)	Metal loading (wt.%)[a]		Average particle size of Au and Cu (nm)[b]
			Au	Cu	
Au/TiO_2	7	Uncalcined	1.729	0	3.1
Cu/TiO_2	7	Uncalcined	0	1.770	1.7
$Au–Cu/TiO_2$	5	Uncalcined	0.892	0.844	3.4
$Au–Cu/TiO_2$	6	Uncalcined	0.896	0.988	2.6
$Au–Cu/TiO_2$	7	Uncalcined	0.980	1.000	2.6
$Au–Cu/TiO_2$	8	Uncalcined	0.693	1.000	2.6
$Au–Cu/TiO_2$	7	473	0.980	1.000	2.4
$Au–Cu/TiO_2$	7	573	0.980	1.000	3.0
$Au–Cu/TiO_2$	7	673	0.980	1.000	3.3
$Au–Cu/TiO_2$[c]	7	Uncalcined	0.980	1.000	3.0

[a] ICP-AES method.
[b] Calculated from TEM data.
[c] After POM reaction at 523 K for 3 h.

of Au in solution was transformed from $AuCl_4^-$ to $Au(OH)_nCl_{4-n}^-$ (n = 1–3) above pH 6. The value of n was closed to 3 at pH 6. At lower pH, there was less hydrolysis of the Au–Cl bond [20]. Similar phenomena have also been applicable for copper nitrate to copper hydroxide. Furthermore, the charge on the TiO_2 surface is also pH dependent. The isoelectric point of Degussa P25 TiO_2 is 6.2–6.4 [21]. Below the isoelectric point (<pH 6.2–6.4) of the support, the surface charge was positive due to the protonation of the surface hydroxyls; above pH 6 the charge was negative due to the removal of protons from the surface hydroxyls. Therefore, electrostatic adsorptions of the gold and copper anions were possible below the IEP value [22]. The adsorption of the negatively charged $Au(OH)_nCl_{4-n}^-$ complex decreases rapidly above the IEP value. In the present study, higher gold uptake was observed at pH 7. However, as the pH increased further, lower uptake of gold was occurred. This can be explained as the surface of the support was negatively charged resulting in an electrostatic repulsion of gold anions at higher pH, and this resulted in the decreased amount of gold uptake at pH 8. These results are in agreement with Moreau and Bond [23], Baatz and Brüße [24], Lee and Gavriilidis [25] and Chang et al. [26].

3.2. XRD

Fig. 1 shows the X-ray diffraction patterns of Au/TiO_2, Cu/TiO_2 and $Au–Cu/TiO_2$ catalysts dried at 373 K. The figure reveals that most of the reflections are from the support TiO_2 (anatase and rutile). The Au/TiO_2 and $Au–Cu/TiO_2$ catalysts showed Au_2O_3 diffraction peak at 2θ = 49.8° (JCPDS 24-0462) (Fig. 1a and c), which proves the existence of oxidic Au species in these samples. The intensity of the oxidic Au peak is smaller in $Au–Cu/TiO_2$ compared to Au/TiO_2 sample. This is because of lesser Au loading in the $Au–Cu/TiO_2$ (1 wt.%) than Au/TiO_2 (2 wt.%). Small intense reflections for metallic gold at 2θ = 38.2° and 44.4° were observed in these catalysts. The low intensity of these peaks may be due to the presence of small gold particles, which are highly dispersed on the support. The peaks correspond to CuO were observed at 35.4°, 38.7°, 44.2° and 61.5° in Cu/TiO_2 and $Au–Cu/TiO_2$ catalysts (Fig. 1b and c). The peak at 44.2° is superimposing with the Au^0 peak at 44.4°. Peaks correspond to Cu_2O and metallic Cu were not observed. This specifies that the particle size of Cu_2O is too small to be detectable by XRD. XPS analysis was subsequently adapted to examine the oxidation state of Au and Cu species at different calcination temperatures and after catalytic test.

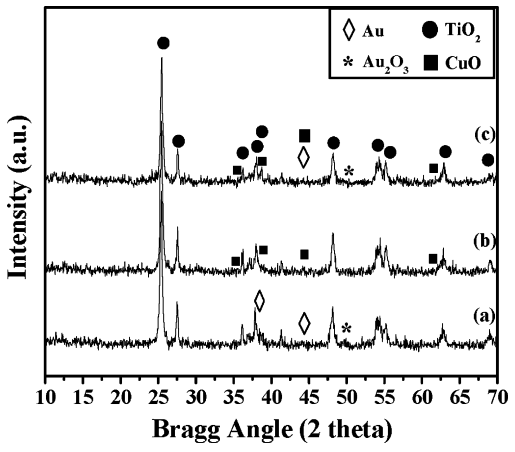

Fig. 1. XRD patterns of: (a) Au/TiO_2 (2 wt.%); (b) Cu/TiO_2 (2 wt.%); (c) $Au–Cu/TiO_2$ (1–1 wt.%) (uncalcined, dried at 373 K; pH, 7).

3.3. TEM

The particle size of gold and copper species in bimetallic $Au–Cu/TiO_2$ catalyst and its corresponding monometallic Au/TiO_2 and Cu/TiO_2 catalysts were examined by TEM analysis. The effect of pH during preparation and effect of calcination temperature on the particle size of Au and Cu in $Au–Cu/TiO_2$ catalyst were also investigated in detail. In addition, to understand the stability of the catalyst during reaction, the particle size of gold and copper in the sample after POM reaction were measured. The results were reported in Table 1. In Au/TiO_2 catalyst, the Au particles were in a wide range of 1.0–4.0 nm. The average size was estimated as 3.1 nm. In Cu/TiO_2 catalyst, the diameter of copper was in the range of 1.0–2.2 nm with a mean diameter of 1.7 nm. For the bimetallic $Au–Cu/TiO_2$ catalyst, since the gold and copper particles are difficult to identify separately in the TEM picture, the particle size of Au and Cu were measured altogether. Major fraction of gold and copper particles is in the range of 1.0–4.0 nm with an average size of 2.6 nm. The particle size of Au and Cu at different pH during preparation of $Au–Cu/TiO_2$ catalyst showed that there was a slight decrease in the average size of gold and copper with increase in pH. At pH 5 the average size of Au and Cu was 3.4 nm. However as the pH is raised, negligible agglomeration occurs, which resulted in smaller metal particles on the support. Therefore at pH between 6 and 8, a uniform size of homogeneously dispersed particle with a mean diameter of 2.6 nm was observed. The main reason for the large sized Au and Cu at lower pH is due to the retention of chlorine and nitrogen in the gold and copper complex ions. For example, the gold precursor ($HAuCl_4$) in water may yield three kinds of possible gold species. At pH 5.5–7.0 most of the Au precursor is present as $AuCl_n(OH)_{4-n}^-$, which can dissolve in water. At pH between 7 and 8, most of the Cl^- ions were displaced by OH^-, leading to a neutrally charged $Au(OH)_3$ species, which precipitates from the solution. Under basic condition the $Au(OH)_3$ dissolve again as $Au(OH)_4^-$. Similar hydrolysis has also been occurred in copper species. The pH of the precipitation solution is very important not only to determine the speciation of $AuCl_n(OH)_{4-n}^-$ and $Cu(NO_3)_n(OH)_{3-n}^-$, but also influences the amount of chloride and nitrate ions adsorbed on the support. The amount of adsorbed chloride and nitrate ions on the support depends on the isoelectric point of the support and its adsorption capacity [27]. At lower pH, the chloride and nitrate ions exist in solution and are apparently more mobile than those at higher pH. They seem to aggregate into larger clusters during drying, resulted in the formation of large sized gold and copper particles. In order to understand the stability of metal particles in the bimetallic $Au–Cu/TiO_2$ catalyst, TEM study was performed at various calcination temperatures and after catalytic test. In uncalcined sample, average particle size was 2.6 nm. After calcination at 473 K, the mean particle size of gold and copper became smaller than those observed in uncalcined sample. In this sample major fraction of gold and copper particles was in the range of 1.0–4.0 nm and exhibited an average particle size of 2.4 nm. Previous studies on supported Au catalysts also showed similar smaller Au particles after calcination at 473 K [19,28]. The reduced size after calcination was explained in terms of conversion of few large-sized oxidized gold species to metallic form. In the sample calcined at 573 K, major fraction of gold and copper particles is in the range of 1.0–5.0 nm with an average value of 3 nm. After calcination at 673 K, although the particle size varied between 2 and 6 nm, most of the particles are in the range of 2.0–5.0 nm. The average particle size was estimated as 3.3 nm. It is noteworthy that the mean size of Au and Cu particles were not affected much even after calcination at 673 K. The particle size of Au in Au/TiO_2 sample was increased from 2.9 to 4.3 nm after calcination at 673 K in our previous study [12]. In the $Au–Cu/TiO_2$ catalyst, presence of copper preserved the Au metal particles dur-

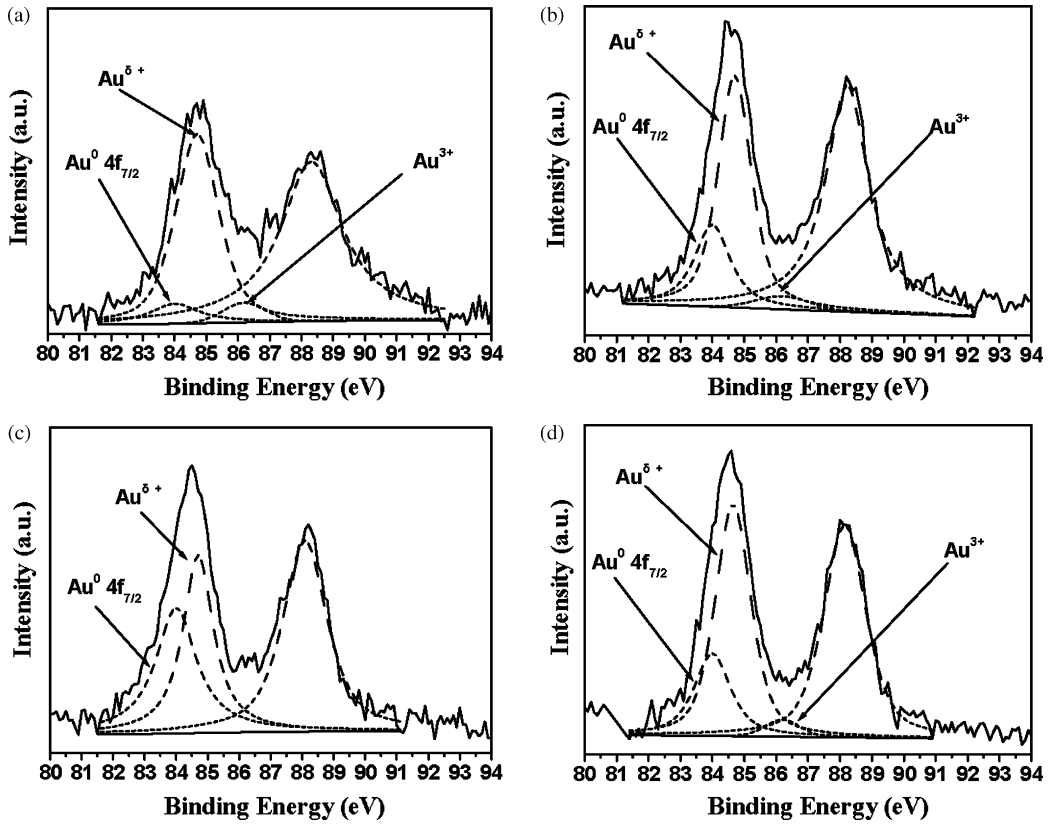

Fig. 2. XPS spectra of Au 4f region for Au–Cu/TiO_2 (1–1 wt.%) catalysts calcined at different temperatures: (a) uncalcined; (b) calcined at 473 K; (c) calcined at 673 K; (d) after POM reaction at 523 K for 3 h.

ing calcination process to a large extent. To understand the particle morphology and particle size of gold and copper in the catalyst sample after POM reaction, the used sample was well-mixed and characterized by TEM technique. It is interesting to note that there was no obvious change in particle size after catalytic test (Table 1). The mean diameter (3 nm) was similar for the sample before and after reaction. There was an increase of Au particle size from 2.9 to 7.4 nm after catalytic test in our previous study on Au/TiO_2 catalyst [12]. This proves that the presence of copper in Au–Cu/TiO_2 catalysts preserved the Au particle size during POM reaction. Therefore, the essential factor of small Au in supported gold catalysts has been fulfilled by the presence of copper species in the catalyst sample.

3.4. XPS

To obtain information on the chemical states of the gold and copper species in Au–Cu/TiO_2 catalysts at different calcination temperatures and after POM reaction, XPS was employed. Fig. 2 compares the XPS spectra of Au 4f core level performed on the Au–Cu/TiO_2 catalyst calcined at different temperatures and after POM reaction at 523 K for 3 h. In the figure, each gold species shows two peaks due to the Au $4f_{7/2}$ and to the Au $4f_{5/2}$ transitions. The XPS spectra of Au 4f level for all samples were deconvoluted into three pairs of peaks with Au $4f_{7/2}$ binding energy 84, 86.2 and 84.7 eV for Au^0, Au^{3+} and $Au^{\delta+}$ species, respectively [29,30]. The corresponding surface distributions of gold and copper species in the catalysts are reported in Table 2. In the uncalcined Au–Cu/TiO_2 sample, there existed $Au^{\delta+}$ (81.6%), Au^{3+} (6.9%) and Au^0 (11.5%) species (Fig. 2a and Table 2). The peaks became sharper and shifted to lower binding energy after calcination process. This suggests that there is a change in the composition of different gold species in the sample. The deconvoluted data in Table 2 shows that the amount of oxidized gold species decreased with consequent increase in the amount of metallic gold species during calcination. Nevertheless, complete reduction of oxidized gold species to metallic gold was not observed as evidenced by the presence of $Au^{\delta+}$ (50.5%) species even after calcination at 673 K (Fig. 2c). Previous literature confirmed that the oxidized gold reduced completely to metallic gold beyond 523 K [31]. This suggests that presence of reducible copper species in Au–Cu/TiO_2 catalysts stabilized the ionic gold species even after calcination at high temperatures. Fig. 2d shows the Au 4f region of the uncalcined Au–Cu/TiO_2 catalyst after POM reaction. In these samples, only few oxidized Au species were reduced to metallic Au (Table 2). Nevertheless, complete reduction of Au species was not observed. Fig. 3 shows the X-ray photoelectron spectra of Cu $2p_{3/2}$ core level for Au–Cu/TiO_2 samples, calcined

Table 2
XPS data of Au 4f and Cu 2p region for different Au–Cu/TiO_2 catalysts

Sample	Au^0 (%)	$Au^{\delta+}$ (%)	Au^{3+} (%)	Cu^0 (%)	Cu_2O (%)	CuO (%)	$Cu(OH)_2$ (%)
Au–Cu/TiO_2 uncalcined	11.5	81.6	6.9	0	62.1	20.3	17.6
Au–Cu/TiO_2 calcined at 473 K	28	67.2	4.8	0	66.1	33.9	0
Au–Cu/TiO_2 calcined at 673 K	49.5	50.5	0	0	63.3	36.7	0
Au–Cu/TiO_2 uncalcined, after POM reaction	27.3	68.6	4.1	13.8	57.9	28.3	0

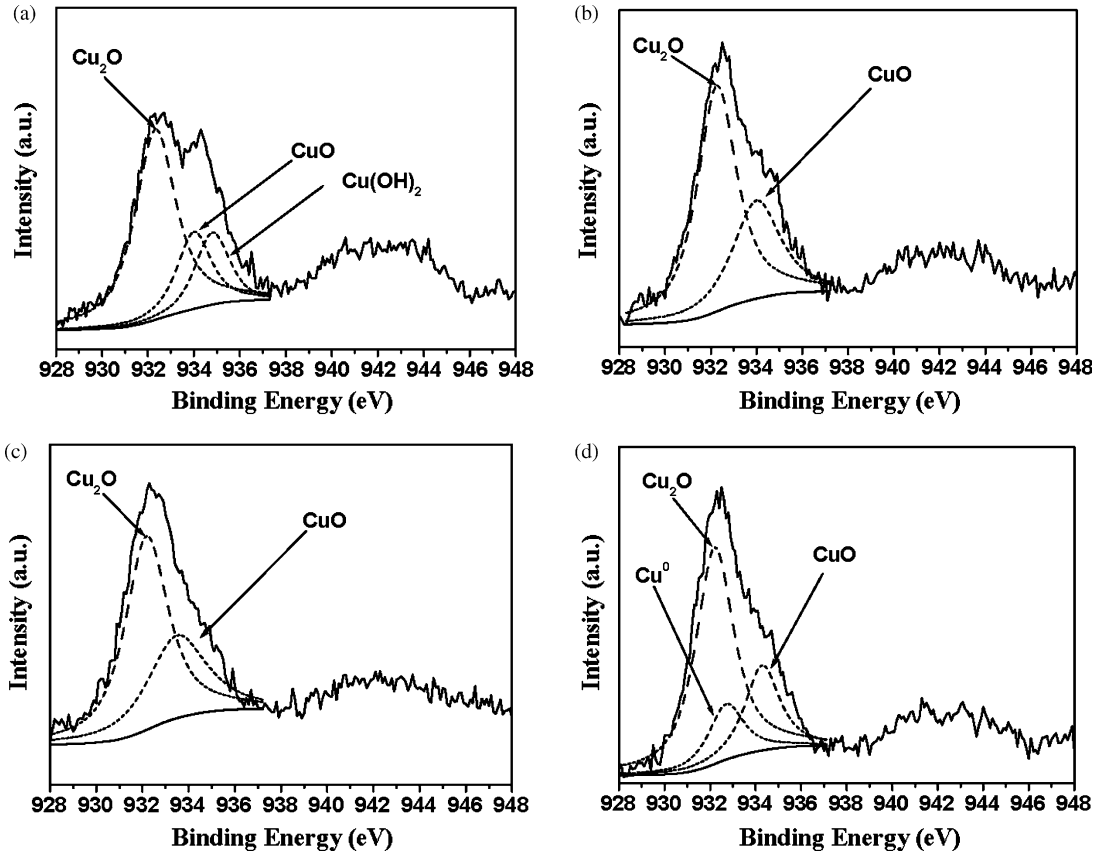

Fig. 3. XPS spectra of Cu 2p region for Au–Cu/TiO_2 (1–1 wt.%) catalysts calcined at different temperatures: (a) uncalcined; (b) calcined at 473 K; (c) calcined at 673 K; (d) after POM reaction at 523 K for 3 h.

at different temperatures along with the spectra recorded for the sample after exposure to POM reaction at 523 K for 3 h. The peaks were deconvoluted for different copper species in the sample. The peaks at 932.3, 932.7, 934 and 934.8 eV were contributed by Cu_2O, Cu^0, CuO and $Cu(OH)_2$, respectively [29,32,33]. The composition of different copper species were given in Table 2. The Cu $2p_{3/2}$ peak of uncalcined sample (Fig. 3a) composed of three main peaks at 932.5, 934 and 934.8 eV, which corresponds to $Cu(OH)_2$, CuO and Cu_2O, respectively. The $Cu(OH)_2$ species was completely disappeared after calcination (Fig. 3b and c). In the uncalcined sample after exposure to POM reaction, the $Cu(OH)_2$ species was completely disappeared and metallic Cu was formed (Fig. 3d). Therefore, metallic Cu, Cu_2O and CuO species were coexisted in the sample after POM reaction. Previous studies on POM over Cu/ZnO catalyst also illustrate the existence of oxidized and reduced copper species on the surface of the catalysts under working conditions during POM reaction [6].

3.5. TPR

TPR technique was employed to gather information on the surface structure and interactions between the metals and the support in Au–Cu/TiO_2 catalyst. Fig. 4 displays the TPR profiles of Au/TiO_2 (2 wt.% Au), Cu/TiO_2 (2 wt.% Cu) and Au–Cu/TiO_2 (1 wt.% Au–1 wt.% Cu) catalysts prepared at pH 7 and were dried in air at 373 K. In all TPR profiles, the reduction process was completed before 435 K. For Au/TiO_2 catalyst, there was no signal for the reduction of oxidized gold species (Fig. 4a). As the oxides of gold in the catalyst are present in small amounts, the hydrogen consumption by the reduction of oxidic Au was less than the detection limit of TCD. The other possibility is that gold is the most electronegative metal and its electron affinity is greater than oxygen. Furthermore, the high value of Au^+/Au^0 couple (+1.691 V) makes the auto-reduction of Au_xO_y before the TPR system getting balanced [34]. Fig. 4b shows the TPR spectrum of Cu/TiO_2 catalyst, the hydrogen consumption of this catalyst is 136.9 μmol/g. The reduction peak at 415 K with a shoulder at 425 K could be assigned to reduction peaks for Cu_2O and CuO to metallic copper, respectively [35]. It agrees with the literature from Gervasini and Bennici [36]. TPR profile of bimetallic Au–Cu/TiO_2 sample showed a single reduction peak at 354 K (Fig. 4c), the consumption of hydrogen for this catalyst is 141.3 μmol/g. This peak was assigned to the reduction of CuO to Cu^0. It is important to note that the presence of gold leads to a considerable lowering

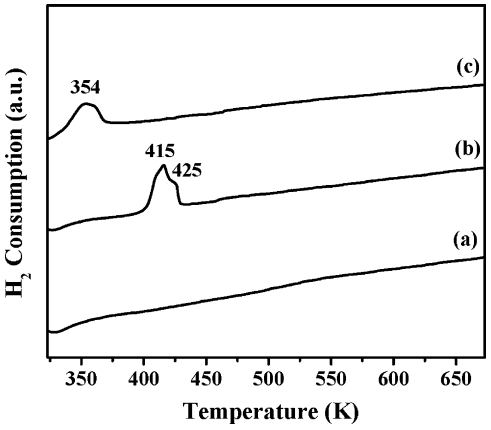

Fig. 4. TPR profiles of: (a) Au/TiO_2 (2 wt.%); (b) Cu/TiO_2 (2 wt.%); (c) Au–Cu/TiO_2 (1–1 wt.%) prepared at pH 7 (uncalcined, dried at 373 K).

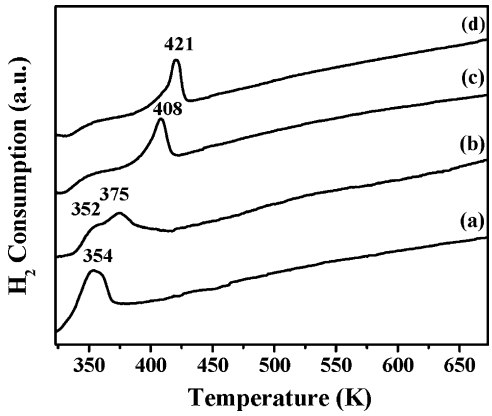

Fig. 5. TPR profiles of Au–Cu/TiO_2 (1–1 wt.%) catalysts calcined at different temperatures: (a) uncalcined; (b) calcined at 473 K; (c) calcined at 573 K; (d) calcined at 673 K (pH, 7).

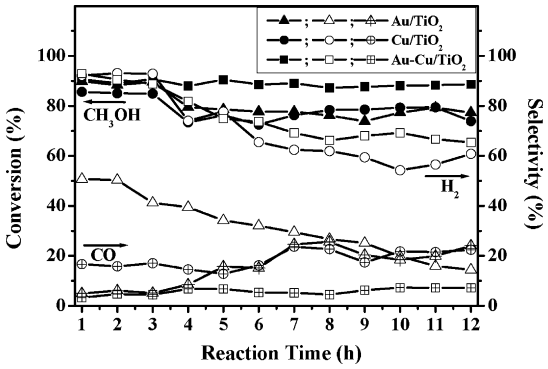

Fig. 6. Catalytic performance of Au/TiO_2, Cu/TiO_2 and Au–Cu/TiO_2 catalysts for CH_3OH conversion, H_2 selectivity and CO selectivity for POM (uncalcined, dried at 373 K; pH, 7; O_2/CH_3OH ratio, 0.3; reaction temperature, 523 K).

of the reduction temperature from the range of 415–425 to 354 K. One possible reason is in the catalyst, gold enhanced the dispersion of CuO thereby preserving smaller CuO particles [37]. Another probable explanation is that gold in the samples could weaken the bond strength of Cu–O and thereby enhanced the reduction of CuO into metallic copper [38]. It leads one to suppose that bimetallic entities are present in all these bimetallic catalysts. Epron et al. [39] observed similar results for the Pt–Cu bimetallic catalyst supported on γ-Al_2O_3. Furthermore, it agrees well with the previous studies on Au/CuO catalysts [16]. Fig. 5 presents the TPR curves of Au–Cu/TiO_2 catalyst sample calcined at different temperatures. The TPR profile of the uncalcined sample (Figs. 4c and 5a) shows a single reduction peak centered at ca. 354 K. The sample calcined at 473 K shows a broad reduction peak at 375 K along with a low temperature shoulder peak at 352 K (Fig. 5b), and the hydrogen consumption of this sample is 125.3 μmol/g. The existence of the two peaks in sample calcined at 473 K might result from the presence of CuO in two different environments, differing in their interaction with the support. One was represented by small CuO particles which were highly dispersed and reduced at lower temperature [37]. Another was represented by large sized CuO particles, which reduced at higher temperature [40]. Fig. 5c and d shows the TPR profiles of the Au–Cu/TiO_2 catalyst calcined at 573 and 673 K, respectively. Both samples showed a single reduction peak. The real hydrogen consumptions for these two catalysts are 67.1 and 66.5 μmol/g, respectively. However, the position of the peak shifted towards higher temperature as the calcination temperature increased. The reduction temperatures were 408 and 421 K for the sample calcined at 573 and 673 K, respectively. The higher reduction temperature indicates the presence of slightly larger CuO crystallites [40]. Robertson et al. [41] and van der Grift et al. [42] studied CuO/SiO_2 catalysts and found that the highly dispersed copper oxide species was more easily reduced than the bulk CuO. Moreover, the reduction peak becomes sharper in the sample calcined at 673 K than those of the sample calcined at 573 K, which indicates the narrower distribution of large sized CuO particles in the sample calcined at 673 K.

3.6. Catalytic activity

The catalytic activity and product distribution in the POM over Au–Cu/TiO_2 catalyst were studied. The activity of Au–Cu/TiO_2 catalyst was compared with Au/TiO_2 and Cu/TiO_2 catalysts. In order to produce highly active catalyst for POM to produce hydrogen, the experimental parameters, such as pH during preparation of the catalysts, calcination temperature and reaction temperature were optimized. The definitions of CH_3OH conversion, O_2 conversion, H_2 selectivity and CO selectivity were listed below:

CH_3OH conversion (%) = (moles of CH_3OH consumed/moles of CH_3OH fed) × 100%;
O_2 conversion (%) = (moles of O_2 consumed/moles of O_2 fed) × 100%;
H_2 selectivity (%) = (moles of H_2 produced × 0.5/moles of CH_3OH consumed) × 100%;
CO selectivity (%) = (moles of CO produced/moles of CH_3OH consumed) × 100%.

The catalytic activity and product distribution in the POM over Au/TiO_2 (2 wt.% Au), Cu/TiO_2 (2 wt.% Cu) and Au–Cu/TiO_2 (1 wt.% Au–1 wt.% Cu) catalysts were compared at 523 K. The product analysis shows that H_2 and CO_2 are the major products and CO and H_2O are the by-products. In addition, traces of HCHO, CH_4 and $HCOOCH_3$ were detected. Fig. 6 shows the CH_3OH conversion, H_2 selectivity and CO selectivity during POM over Au/TiO_2, Cu/TiO_2 and Au–Cu/TiO_2 catalysts. The bimetallic Au–Cu/TiO_2 catalysts showed higher activity in terms of methanol conversion and hydrogen selectivity than the monometallic Au/TiO_2 and Cu/TiO_2 catalysts. Concerning the stability of the catalysts, there was a slight decrease in CH_3OH conversion with reaction time in both monometallic catalysts. It is noteworthy that the bimetallic catalysts showed stable methanol conversion for 12 h. The Au/TiO_2 catalyst exhibited low H_2 selectivity and it decreased with reaction time. The Cu/TiO_2 and Au–Cu/TiO_2 catalysts showed high H_2 selectivity and it decreased with reaction time. The decrease was much higher in Cu/TiO_2 catalyst than Au–Cu/TiO_2 catalyst. The main disadvantage of Cu/TiO_2 catalyst is that the catalyst produced high CO as by-product. The bimetallic catalyst showed much lower CO selectivity throughout the long catalytic run. The Cu/TiO_2 catalyst showed higher CO selectivity compared to Au–Cu/TiO_2 catalyst. Previous studies also showed a similar higher CO selectivity in Cu/ZnO catalysts [6,9]. In Au/TiO_2 catalyst, the CO selectivity was lower at the beginning, but a significant increase was observed with reaction time. The higher CO selectivity was due to agglomeration of Au nano-particles with reaction time, which resist the secondary favorable reaction such as, CO oxidation and water gas shift. However, this type of Au particle growth was not expected in Au–Cu/TiO_2 catalyst, where copper species preserved the Au particle growth (Table 1). The high activity, selectivity and stability of the bimetallic catalyst, correlate closely to the charge transfer in metal–metal species, which increase the availability of reactive oxygen. Recalling the experimental data of TPR in Fig. 4, the Au–Cu/TiO_2 catalyst displayed lowest reduction

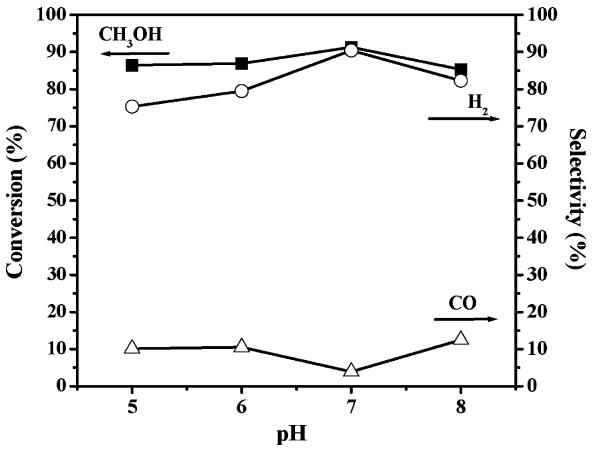

Fig. 7. Effect of pH on CH_3OH conversion, H_2 selectivity and CO selectivity for POM over Au–Cu/TiO_2 (1–1 wt.%) catalysts (uncalcined, dried at 373 K; O_2/CH_3OH ratio, 0.3; reaction temperature, 523 K; reaction time, 90 min).

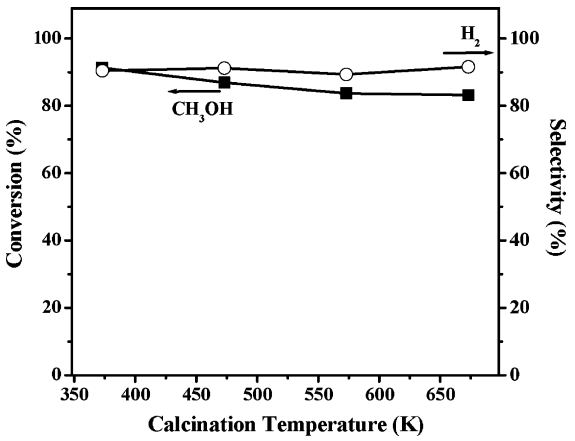

Fig. 8. Effect of calcination temperature on CH_3OH conversion and H_2 selectivity for POM over Au–Cu/TiO_2 (1–1 wt.%) catalysts (pH, 7; O_2/CH_3OH ratio, 0.3; reaction temperature, 523 K; reaction time, 90 min).

temperature for the reduction of copper oxide compared to Cu/TiO_2. This indicates the presence of small CuO particle in the bimetallic system and hence a higher dispersion of the catalyst. This suggests large interfacial area resulting from nano-size Cu or Au clusters enables electronic and chemical interactions between the two metals to occur to a large extent [43]. The interaction of gold with copper facilitates the activation of sites due to change of redox and electronic properties of gold species [13]. Pestryakov et al. [44] reported that the dispersed particles of gold are oxidized easier than large aggregates. In our study, XPS analysis revealed the presence of copper in Au–Cu/TiO_2 catalysts stabilized the ionic gold species ($Au^{\delta+}$) during calcination and after catalytic run (Fig. 2 and Table 2). The ionic gold species has been suggested as an active component for supported gold catalysts [20]. Liu [43] proposed a unified mechanistic model for a chemical reaction. According to this model, there was a transfer of oxygen atom from one molecule to another in chemical reaction. This suggests that in supported gold catalysts containing copper species, small gold particles were stabilized, which consequently increase the ionic gold species by O_2 activation. This activation is related to the ability of the copper species in supplying the active oxygen during the catalytic reaction. The oxygen vacancy created on copper can be filled by O_2 from the feed and again leave activated oxygen on the surface. The highly reactive oxygen further involves in the POM and produce hydrogen. These processes are continuing during the reaction and facilitating stable activity. Therefore, the enhanced activity, selectivity and stability of the bimetallic catalysts are due to metal–metal interaction. This interaction caused by the redox properties of Cu, which stabilize the active $Au^{\delta+}$ species and also stabilize the Au particle size.

Fig. 7 shows the catalytic activity of Au–Cu/TiO_2 catalyst prepared at different pH. It reveals that the methanol conversion increased with increase in pH and reached a maximum at pH 7, thereafter it decreased. The H_2 selectivity was also increased with increase in pH and it dropped at pH 8. The behavior of the catalysts prepared at various pH in methanol conversion and H_2 selectivity were explained in terms of amount of Au and Cu deposited on TiO_2 and the mean particle size of Au and Cu at various pH values. The pH of preparation has the remarkable influence on the particle size of Au and Cu and metal loading (Table 1). The lower activity at pH 5 has been explained in terms of presence of large sized Au and Cu particles and lower Au and Cu loadings on the support. The selectivity towards CO was decreased with rise in pH from 5 to 6 and reached a minimum at pH 7 and then increased continuously with rise in pH. At pH 7, high CH_3OH conversion and H_2 selectivity with lesser amount of CO was observed. This is due to higher Au and Cu loadings and smaller Au and Cu particles in these catalysts. Similar effects of pH on gold particle size, gold uptake and catalytic activity was reported in the literuature [20,45]. Since the catalyst prepared at pH 7 exhibited higher methanol conversion and hydrogen selectivity with smaller CO selectivity, the catalyst samples prepared at pH 7 has been used for further study.

Fig. 8 demonstrates the effect of calcination temperature on the catalytic activity of Au–Cu/TiO_2 catalysts prepared at pH 7. With increasing calcination temperature, a slight decrease in CH_3OH conversion was observed. On the other hand, there was no significant change in hydrogen selectivity. In our previous study on Au/TiO_2–Fe_2O_3 catalyst, a considerable decrease in H_2 selectivity with rise in calcination temperature was observed, which was due to the absence of $Au^{\delta+}$ species [19]. Guzman and Gates [46] found that the supported gold catalysts displayed well in CO oxidation contained $Au^{\delta+}$ species and they proposed these species as catalytic sites in the catalysts. Concurrently, particle size of Au also plays an important role in determining the activity of the catalyst, with small gold particles exhibit higher catalytic activity. In the present study, TEM and XPS studies were undertaken for the Au–Cu/TiO_2 sample calcined at different temperatures to find out the active component in the catalyst. TEM analysis revealed that the size of the Au and Cu particles was not affected much with calcination temperature. This suggests that the presence of copper particles preserves the Au particle size during calcination process to a large extent. XPS analysis illustrates that the catalyst is composed of Au^0, Au^{3+} and $Au^{\delta+}$ species with varying amount at different calcination temperatures. The active component for supported gold catalyst, i.e. $Au^{\delta+}$ species is noticeably present even in the sample calcined at 673 K. Therefore, the presence of easily reducible copper species in Au–Cu/TiO_2 catalyst not only stabilized the Au particle size but also preserved the active component in the catalyst during calcination process. This arises by chemical interaction between Au and Cu species. TPR analysis clearly proves the interaction between Au and Cu. Nevertheless, the small decrease in activity in terms of methanol conversion with calcination temperature has to taken into consideration to find out the cause for this decrease in activity. The uncalcined catalyst shows slightly larger particles compared to the one calcined at 473 K (Table 1). This suggests that particle size of Au was not the cause for this decrease. XPS analysis shows that the uncalcined sample mainly composed of oxidized gold species preferably the $Au^{\delta+}$ species, which is the active component for supported gold catalysts. With increasing calcination temperature, the oxidized gold species partially reduced to metallic Au. The sample

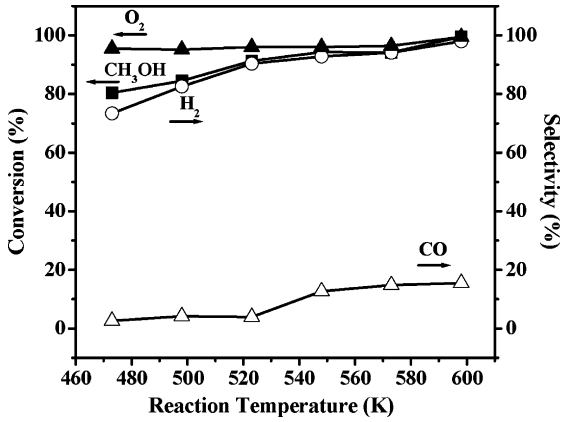

Fig. 9. Effect of reaction temperature on CH_3OH conversion, O_2 conversion, H_2 selectivity and CO selectivity for POM over Au–Cu/TiO_2 (1–1 wt.%) catalysts (uncalcined, dried at 373 K; pH, 7; O_2/CH_3OH ratio, 0.3; reaction time, 90 min).

after calcination at 673 K is mainly composed of Au^0 (49.5%) and $Au^{\delta+}$ (50.5%) species (Table 2). Therefore, it is suggested that the slight decrease in activity with calcination temperature is caused by the presence of comparatively lesser amount of oxidized gold species ($Au^{\delta+}$) in the catalyst sample. The active component in the catalyst is not completely reduced to metallic Au even after calcination at 673 K and these catalysts exhibited good activity for POM reaction. Since the Au–Cu/TiO_2 catalyst sample without calcination itself showed better performance in POM to produce hydrogen, this catalyst has been used for further studies.

Fig. 9 presents the CH_3OH conversion, O_2 conversion, H_2 selectivity and CO selectivity for POM over Au–Cu/TiO_2 catalysts at reaction temperatures between 473 and 598 K. The O_2 conversion was 95.5% at 473 K, and it increased with increasing reaction temperature and reached 99.5% at 598 K. The CH_3OH conversion and H_2 selectivity were increased from 80.4 to 99.6 and 73.4 to 98%, respectively when the temperature increased from 473 to 598 K. The lower H_2 selectivity at 473 K indicates that methanol combustion (MC) has taken place along with POM and produce H_2O and CO_2 (Eq. (2)) [47]. Nevertheless, the involvement of MC was very less compared to POM:

$$CH_3OH + 1.5O_2 \rightarrow 2H_2O + CO_2 \quad (2)$$

When the temperature increased from 498 to 523 K, significant increase in H_2 selectivity (82.6–90.4%) was observed. This could be regarded as the steam reforming reaction (SRM) was occurred (Eq. (3)). The H_2O formed in the MC was used by SRM reaction, thereby increased H_2 selectivity. The SRM can be considered as a combination of WGS reaction (Eq. (4)) and methanol decomposition (MD) (Eq. (5)) [48]:

$$CH_3OH + H_2O \rightarrow 3H_2 + CO_2 \quad (3)$$

$$CO + H_2O \leftrightarrow CO_2 + H_2 \quad (4)$$

$$CH_3OH \rightarrow CO + 2H_2 \quad (5)$$

There was a considerable increase in CO selectivity at 548 K. This result suggests that when the reaction temperature ≥548 K, the unfavorable reactions such as, methanol decomposition and/or reverse water gas shift (RWGS) were occurred [10]. Previous reports evidenced the initiation of MD beyond 523 K [19,49,50]. Nevertheless, the CO selectivity keeps nearly a steady value between 548 and 598 K. This relates to the participation of CO oxidation (Eq. (6)) and/or WGS (Eq. (4)) reactions:

$$CO + 0.5O_2 \rightarrow CO_2 \quad (6)$$

However, the presence of significant amount of CO (∼15%) at high temperatures implied that the reaction rate of MD is faster than CO oxidation and WGS reactions. Thus, the overall reactions involved at different reaction temperatures are suggested as MC, POM, SRM, MD, RWGS, WGS and CO oxidation.

4. Conclusions

The present study demonstrates that the bimetallic Au–Cu/TiO_2 catalysts are highly active, stable and selective towards hydrogen in comparison to its corresponding monometallic Au/TiO_2 and Cu/TiO_2 catalysts. This could be explained in terms of metal–metal interaction that creates smaller metal particles and preserved the active component in supported gold catalysts. The optimum pH for preparing the high active Au–Cu/TiO_2 catalysts was pH 7. The catalyst preparation and reaction conditions for the bimetallic Au–Cu/TiO_2 catalysts were optimized. There was only a slight decrease in activity with increase in calcination temperature. This was due to the stabilization of small Au particles and ionic gold species. The catalytic performance at various reaction temperatures in the range of 473–598 K showed that at 523 K, the catalyst exhibited higher CH_3OH conversion, H_2 selectivity with smaller CO selectivity.

Acknowledgement

The authors express thanks to the Ministry of Economical Affairs of Taiwan for its financial support under contract number 94-EC-17-A-09-S1-022.

References

[1] N. Edwards, S.R. Ellis, J.C. Frost, S.E. Golunski, A.N.J. Keulen, N.G. Lindewald, J.G. Reinkingh, J. Power Sources 71 (1998) 123–128.
[2] T. Shishido, Y. Yamamoto, H. Morioka, K. Takehira, J. Mol. Catal. A 268 (2007) 185–194.
[3] P.J. de Wild, M.J.F.M. Verhaak, Catal. Today 60 (2000) 3–10.
[4] M.L. Cubeiro, J.L.G. Fierro, Appl. Catal. A 168 (1998) 307–322.
[5] M.L. Cubeiro, J.L.G. Fierro, J. Catal. 179 (1998) 150–162.
[6] J. Agrell, K. Hasselbo, K. Jansson, S.G. Jaras, M. Boutonnet, Appl. Catal. A 211 (2001) 239–250.
[7] S. Murcia-Mascaros, R.M. Navarro, L. Gomez-Sainero, U. Costantino, M. Nocchetti, J.L.G. Fierro, J. Catal. 198 (2001) 338–347.
[8] G.S. Wu, L.C. Wang, Y.M. Liu, Y. Cao, W.L. Dai, H.Y. He, K.N. Fan, Appl. Surf. Sci. 253 (2006) 974–982.
[9] L. Alejo, R. Lago, M.A. Peña, J.L.G. Fierro, Appl. Catal. A 162 (1997) 281–297.
[10] R. Ubago-Pérez, F. Carrasco-Marín, C. Moreno-Castilla, Catal. Today 123 (2007) 158–163.
[11] G.J. Hutchings, Catal. Today 100 (2005) 55–61.
[12] F.-W. Chang, H.-Y. Yu, L.S. Roselin, H.-C. Yang, Appl. Catal. A 290 (2005) 138–147.
[13] E. Smolentseva, N. Bogdanchikova, A. Simakov, A. Pestryakov, I. Tusovskaya, M. Avalos, M.H. Farías, J.A. Díaz, V. Gurin, Surf. Sci. 600 (2006) 4256–4259.
[14] S.D. Lin, A.C. Gluhoi, B.E. Nieuwenhuys, Catal. Today 90 (2004) 3–14.
[15] A. Venugopal, J. Aluha, M.S. Scurrel, Catal. Lett. 90 (2003) 1–6.
[16] B.E. Solsona, T. Garcia, C. Jones, S.H. Taylor, A.F. Carley, J. Graham, Hutchings, App. Catal. A 312 (2006) 67–76.
[17] R.J. Chimentão, F. Medina, J.L.G. Fierro, J. Llorca, J.E. Sueiras, Y. Cesteros, P. Salagre, J. Mol. Catal. A 274 (2007) 159–168.
[18] P. Haider, A. Baiker, J. Catal. 248 (2007) 175–187.
[19] F.-W. Chang, H.-Y. Yu, L.S. Roselin, H.-C. Yang, T.-C. Ou, Appl. Catal. A 302 (2006) 157–167.
[20] M. Haruta, Catal. Today 36 (1997) 153–166.
[21] R.R. Bacsa, J. Kiwi, Appl. Catal. B 16 (1998) 19–29.
[22] S. Ivanova, V. Pitchon, C. Petit, J. Mol. Catal. A 256 (2006) 278–283.
[23] F. Moreau, G.C. Bond, Catal. Today 122 (2007) 260–265.
[24] C. Baatz, U. Brüße, J. Catal. 249 (2007) 34–40.
[25] S. Lee, A. Gavriilidis, J. Catal. 206 (2002) 305–313.
[26] C.K. Chang, Y.J. Chen, C.T. Yeh, Appl. Catal. A 174 (1998) 13–23.
[27] S. Wang, T. Zhang, X. Wang, S. Zhang, S. Wang, W. Huang, S. Wu, J. Mol. Catal. A 272 (2007) 45–52.
[28] A. Wolf, F. Schuth, Appl. Catal. A 226 (2002) 1–13.
[29] J.F. Moulder, W.F. Stickle, P.E. Sobol, K.D. Bomben, J. Chastain, R.C. King Jr., Handbook of X-ray Photoelectron Spectroscopy, Physical Electronics, Inc., Eden Prairie, MN, 1992.

[30] A.M. Visco, F. Neri, G. Neri, A. Donato, C. Milone, S. Galvagno, Phys. Chem. Chem. Phys. 1 (1999) 2869–2873.
[31] X. Xu, J. Li, Z. Hao, W. Zhao, C. Hu, Mater. Res. Bull. 41 (2006) 406–413.
[32] Z. Mekhalif, F. Sinapi, F. Laffineur, J. Delhalle, J. Electron Spectrosc. Relat. Phenom. 121 (2001) 149–161.
[33] R.G. Herman, K. Klier, G.W. Simmons, P.B. Finn, J.B. Bulko, T.P. Kobylinski, J. Catal. 56 (1979) 407–429.
[34] G.C. Bond, D.T. Thompson, Catal. Rev. Sci. Eng. 41 (1999) 319–388.
[35] G. Águila, F. Gracia, J. Cortés, P. Araya, Appl. Catal. B 77 (2008) 325–338.
[36] A. Gervasini, S. Bennici, Appl. Catal. A 281 (2005) 199–205.
[37] J. Agrell, M. Boutonnet, I.M. Cabrera, J.L.G. Fierro, Appl. Catal. A 253 (2003) 201–211.
[38] H.L. Lian, M.J. Jai, W. Zhang, D. Jiang, Chem. Res. Chin. U 22 (2006) 99–102.
[39] F. Epron, F. Gauthard, J. Barbier, Appl. Catal. A 237 (2002) 253–261.
[40] J. Xiaoyuan, L. Guanglie, Z. Renxian, M. Jianxin, C. Yu, Z. Xiaming, Appl. Surf. Sci. 173 (2001) 208–220.
[41] S.D. Robertson, B.D. Mcnicol, J.H. de Baas, S.C. Kloet, J. Catal. 37 (1975) 424–431.
[42] C.J.G. van der Grift, A.F.H. Wielers, B.P.J. Jogh, J. Van Beunum, M. De Boer, M. Versluijs-Helder, J.W. Geus, J. Catal. 131 (1991) 178–189.
[43] W. Liu, Chem. Eng. Sci. 62 (2007) 3502–3512.
[44] A.N. Pestryakov, V.V. Luninb, A.N. Kharlanovb, D.I. Kochubeyc, N. Bogdanchikovad, A.Yu. Stakheev, J. Mol. Struct. 642 (2002) 129–136.
[45] C. Cellier, S. Lambert, E.M. Gaigneaux, C. Poleunis, V. Ruaux, P. Eloy, C. Lahousse, P. Bertrand, J.-P. Pirard, P. Grange, Appl. Catal. B 70 (2007) 406–416.
[46] J. Guzman, B.C. Gates, J. Am. Chem. Soc. 126 (2004) 2672–2673.
[47] J. Agrell, M. Boutonnet, J.L.G. Fierro, Appl. Catal. A 253 (2003) 213–223.
[48] J. Agrell, H. Birgersson, M. Boutonnet, I. Melián-Cabrera, R.M. Navarro, J.L.G. Fierro, J. Catal. 219 (2003) 389–403.
[49] H.-C. Yang, F.-W. Chang, L.S. Roselin, J. Mol. Catal. A 276 (2007) 184–190.
[50] F.-W. Chang, L.S. Roselin, T.-C. Ou, Appl. Catal. A 334 (2008) 147–155.